Research Square

Preprints are preliminary reports that have not undergone peer review.
They should not be considered conclusive, used to inform clinical practice,
or referenced by the media as validated information.

Effect of Welding Groove Geometry on the Microstructure, Mechanical Properties and Ballistic Performance of 20-mm M450 Armor Steel

Müesser Göçmen
İstanbul Gedik University: T C Istanbul Gedik Universitesi
Ozan Coban
ozan.coban@gedik.edu.tr
İstanbul Gedik University: T C Istanbul Gedik Universitesi https://orcid.org/0000-0002-1506-4619
Mustafa Koçak
İstanbul Gedik University: T C Istanbul Gedik Universitesi
Uğur Gürol
FOSECO Foundry

Research Article

Keywords: armor steel, HSLA steel, heat-affected zone, microstructure, mechanical properties, ballistic performance

Posted Date: September 28th, 2026

DOI: https://doi.org/10.21203/rs.3.rs-10856179/v1

License: This work is licensed under a Creative Commons Attribution 4.0 International License.
Read Full License

Abstract

The effect of welding groove geometry on the microstructure, mechanical properties, and ballistic performance of armor-steel was investigated. Four different groove configurations, namely single-V, double-V, single-bevel, and double-bevel, were prepared and welded using robotic gas metal arc welding (GMAW) with ER110 SG ferritic filler wire. Macrostructural and microstructural characterization, hardness measurements, tensile testing, impact testing at − 40°C, and ballistic testing were conducted. The results demonstrated that groove geometry significantly influenced the thermal history, microstructural evolution, and mechanical response of the welded joints. The double-bevel configuration exhibited the highest average tensile strength of 959 MPa, whereas the double-V configuration provided the most balanced combination of strength and ductility, with 932 MPa tensile strength. The double-V geometry also produced the lowest softening in both the weld metal and heat-affected zone (HAZ). Weld-metal hardness ranged from 277.5 to 303.7 HV, while HAZ hardness ranged from 290.6 to 312.8 HV. The weld metal consisted predominantly of fine acicular and polygonal ferrite. The single-V joint showed the coarsest M-A constituent morphology in the central ICHAZ, whereas the double-V joint exhibited the finest morphology and highest local hardness. The highest weld-metal and HAZ toughness values were obtained for the single-V (69 J) and single-bevel (145 J) joints, respectively. All ballistic impacts resulted in partial penetration/deformation without complete perforation. The single-bevel and double-V geometries exhibited the lowest HAZ penetration depths, consistent with their narrower softening zones. Overall, welding groove geometry was identified as a critical design parameter governing the local ballistic resistance of armor-steel joints.

1. Introduction

Armor steels are widely used in military vehicles and other protective structures because of their combination of high hardness, high strength, and sufficient toughness, which enables them to resist projectile impact while maintaining structural integrity. However, the complex geometries and large dimensions of armored vehicle structures generally prevent the use of monolithic components, making welding an essential manufacturing route. Consequently, the ballistic and structural performance of an armored structure is determined not only by the properties of the base armor steel but also by the metallurgical, mechanical, and geometric integrity of its welded joints [1–5].

Gas metal arc welding (GMAW), particularly metal active gas (MAG) welding, is frequently employed for the fabrication of armor-steel structures because of its high deposition rate, relatively high welding speed, process flexibility, and suitability for mechanized and robotic production [4, 6–9]. Nevertheless, the welding thermal cycle can substantially modify the microstructure and hardness of high-strength armor steels. The heat-affected zone (HAZ) can be divided into several characteristic subregions, including the coarse-grained HAZ (CGHAZ), fine-grained HAZ (FGHAZ), intercritical HAZ (ICHAZ), and subcritical HAZ (SCHAZ), each of which experiences a different peak temperature and cooling history. Consequently, pronounced spatial variations in phase constitution, hardness, toughness, and fracture resistance may develop across the HAZ [2, 10, 11]. HAZ softening is therefore one of the major

metallurgical concerns in welding quenched-and-tempered armor steels, particularly because local reductions in hardness can adversely affect ballistic resistance [2, 10, 12].

The welding thermal cycle and filler-metal composition are among the principal factors governing the microstructure and mechanical performance of armor-steel joints [6–9, 13–16]. The selection of the filler metal is particularly important because the resulting weld-metal chemistry, strength mismatch, phase constitution, and hardness can significantly influence the overall response of the joint. Austenitic filler metals are often selected because of their high ductility and toughness, whereas ferritic high-strength fillers can provide greater weld-metal hardness and strength [6, 7, 13, 14]. Recent robotic-MAG investigations have demonstrated that ferritic ER110-type filler metals can produce relatively hard weld metals with acicular-ferrite- and bainite-related microstructures, while austenitic and duplex fillers can provide higher low-temperature impact toughness [7]. Similar trends have been reported for armor-steel joints welded with different consumables, confirming the strong relationship between filler-metal chemistry, weld-metal microstructure, and mechanical performance [13–16]. The microstructural heterogeneity generated within the HAZ is also of particular importance. Partial austenitization in the ICHAZ can lead to the formation of martensite–austenite (M-A) constituents within a softened matrix, while repeated thermal cycling during multipass welding can further modify previously formed microstructures [10, 11, 17, 18]. The morphology, size, and distribution of M-A constituents can act as local stress concentrators and influence both hardness and toughness. In the weld metal, the relative proportions of acicular ferrite, polygonal ferrite, bainitic structures, and M-A constituents can similarly affect the balance between strength and impact toughness [7, 13, 15, 17]. Therefore, the thermal history associated with multipass welding must be considered together with nominal heat input when evaluating the performance of armor-steel joints.

The effects of welding thermal conditions on ballistic performance have been demonstrated in several studies. Savic and Cabrilo [19] showed that the ballistic resistance of the HAZ in robot-controlled GMAW armor-steel weldments was strongly affected by heat input, with the lower-heat-input condition exhibiting greater resistance to projectile penetration. Souza et al. [20] likewise demonstrated that changes in heat input resulted in substantial microstructural differences and corresponding changes in the ballistic performance of welded high-hardness armor steel. Other investigations have shown that the weld-metal microstructure, strength mismatch, hardness distribution, filler-metal type, and local failure mechanisms can influence the ballistic response of welded armor-steel joints [5, 21–23]. For example, the ballistic behavior of ARMOX 500T welded joints has been shown to depend on filler-metal hardness and welding sequence [5], while GMAW-welded dissimilar armor-steel joints have exhibited different ballistic failure modes depending on the filler-metal system and local weld-metal properties [21].

Although the effects of welding process, heat input, and filler-metal selection on armor-steel weldments have been extensively investigated, the influence of welding groove geometry remains comparatively less explored, particularly when microstructural, mechanical, and ballistic performance are considered simultaneously. Groove geometry directly affects the weld-metal volume, number and sequence of welding passes, heat dissipation characteristics, thermal cycling of the HAZ, and resulting hardness

distribution. Studies on quenched-and-tempered steels have demonstrated that groove design can significantly influence heat dissipation, microhardness, tensile properties, and impact toughness, with double-V configurations exhibiting particularly favorable strength characteristics in some conditions [24]. In armor-steel welding, İpek and Elaldi [25] investigated V- and X-groove configurations at different groove angles and demonstrated that both groove geometry and groove angle affected tensile, compressive, and bending strength. These results indicate that groove geometry is not merely a geometric parameter for controlling weld-metal volume but can also modify the thermal and mechanical response of the resulting joint.

Nevertheless, the available literature on armor-steel groove geometry remains concentrated mainly on conventional V- and X-type configurations and, in some cases, narrow-gap welding. Kim and Yi [26] compared narrow-gap GMAW with a conventional X-groove configuration for armor steel and reported differences in mechanical properties and residual stress distribution. Other studies have investigated the effect of groove preparation and groove-surface condition on the metallurgical and mechanical properties of armor-steel weldments [27]. However, systematic comparisons involving a broader range of conventional groove configurations, particularly single-bevel and double-bevel geometries, remain scarce. More importantly, the direct relationship between groove geometry and ballistic resistance has received very limited attention. To the best of the authors' knowledge based on the literature identified in this study, Kim and Yi [26] represent the only previously identified investigation that directly compared different groove configurations in armor-steel welding while also incorporating ballistic testing. In that work, narrow-gap and conventional X-groove joints were evaluated, and ballistic testing was used to verify the protection capability of the welded joint [26].

Thus, while groove geometry has been investigated in relation to tensile strength, hardness, impact toughness, residual stress, and weldability, its direct relationship with local projectile penetration behavior remains largely unexplored. This gap is particularly important for thick armor plates, where groove geometry controls not only the amount of deposited weld metal but also the number and sequence of welding passes and, consequently, the thermal cycling imposed on the surrounding HAZ. Such differences can modify the extent of HAZ softening and the local resistance of the welded joint to projectile penetration. A joint may therefore exhibit adequate or even high tensile strength while simultaneously developing a relatively wide softened HAZ that becomes more susceptible to localized projectile penetration [19–23]. Accordingly, evaluating groove geometry solely through conventional mechanical properties may not adequately describe the ballistic reliability of armor-steel weldments. A systematic comparison of different groove configurations using both mechanical and ballistic characterization is therefore required.

Therefore, the objective of the present study was to systematically investigate the effect of four different welding groove geometries—single-V, double-V, single-bevel, and double-bevel—on the microstructure, hardness distribution, tensile properties, impact toughness, and ballistic performance of 20-mm-thick M450 armor steel welded using the GMAW process and ER110 SG filler metal. The principal novelty of the study lies in establishing a direct relationship between groove geometry, welding thermal conditions,

HAZ softening, microstructural evolution, mechanical performance, and local ballistic penetration behavior. In particular, the study provides a comparative assessment of Depth of Penetration (DoP) and Width of Penetration (WoP) in both the weld metal and HAZ, thereby enabling the effect of groove geometry on localized ballistic response to be evaluated alongside conventional mechanical and microstructural characteristics.

2. Materials and Experimental Procedure

2.1. Base Material and Filler Metal

A 20-mm-thick M450 armor steel (MIL-DTL-46100 Class 2) produced by Miilux Oy was used as the base material, and a 1.2-mm-diameter ER110 SG high-strength GMAW wire manufactured by Gedik Welding Company was used as the filler metal. The chemical compositions of base material and filler metal were presented in Table 1.

Table 1
Chemical composition of M450 armor steel (base material) and ER 110 SG filler metal

M450 Armor Steel	**C**	**Si**	**Mn**	**Cr**	**Ni**	**Mo**	**P**	**S**	**Ceq**
	0.26	**0.7**	**1.7**	**1.3**	**0.8**	**0.5**	**0.025**	**0.01**	**0.63**
GekaTec ER 110 SG Filler Metal	0.07	0.40	1.20	0.31	1.56	0.28			

The mechanical properties of base material and filler metal were presented in Table 2. According to the manufacturer's data, the filler metal has a minimum yield strength of 690 MPa, a tensile strength of 770–940 MPa, a minimum elongation of 17%, and a Charpy impact toughness of 47 J at − 40°C. According to the yield strength values, the joint efficiency was expected to be approx. 58,62% which reveals an undermatching design.

Table 2
Mechanical properties of M450 armor steel (base material) and ER 110 SG filler metal

Material	**Yield strength (MPa)**	**Tensile strength (MPa)**	**Elongation (%)**	**Charpy impact toughness at − 40°C (J)**
M450 armor steel	1177	1514	11	23
GekaTec ER 110 SG	min.690	770–940	min.17	47

2.2. Groove Geometries and Welding Procedure

Four groove geometries were investigated; single-V (V), double V (X), double-bevel (K), and single-bevel (I/). All groove configurations were prepared with a constant groove angle of 30° according to EN ISO

9692-1. A 5-mm root gap was used, and the plate edges were prepared with a 2-mm chamfer. Weld groove configuration was shown in Fig. 1.

Before welding, the residual magnetic field of the plates was measured because residual magnetism can cause arc blow and adversely affect arc stability. Where necessary, demagnetization was performed. The plates were preheated to 120 ± 10°C using a propane torch. The maximum interpass temperature was controlled below 150°C.

All joints were produced using a Gekamac Power MIG GPS WB P500L welding machine. The shielding gas was an M21 gas mixture containing 82% Ar and 18% CO_2, with a flow rate of 15 L/min., in accordance with EN ISO 14175. The welding parameters are summarized in Table 3.

Table 3
Welding parameters used for the different groove geometries

Groove geometry	Current (A)	Voltage (V)	Welding speed (cm/min)	Heat input (kJ/mm)
Single-V (V)	250	30	30.7	1.10
Double-V (X)	250	30	34.0	1.10
Double-bevel (K)	228	30	34.0	1.08
Single-bevel (I/)	224	30	34.0	1.07

The single-V joint was deposited using six layers and 14 passes. The double-V joint was produced using six layers and nine passes, while the double-bevel and single-bevel joints were welded using six layers and nine and ten passes, respectively.

2.3. Metallographic Characterization

Cross-sectional specimens were prepared by sequential grinding using abrasive papers from 80 to 2500 grit, followed by polishing with a 3-μm alumina suspension. The specimens were etched using a 10% nital solution. Macrostructural examination was conducted according to EN ISO 17639. Optical microscopy was used to characterize the weld metal, fusion boundary, CGHAZ, FGHAZ, ICHAZ, and SCHAZ. Detailed microstructural observations were performed using a FEI Quanta FEG 450 scanning electron microscope.

2.4. Mechanical Testing

Mechanical test specimens were extracted from the welded test pieces in accordance with the requirements of EN ISO 15614-1. Tensile specimens were extracted transversely from each welded plate and tested according to EN ISO 4136. Two tensile specimens were tested for each groove geometry. Charpy V-notch impact specimens were extracted from the weld metal and HAZ. The impact tests were performed at − 40°C. Hardness measurements were conducted according to EN ISO 6507-1 using a HV5 load. Hardness profiles were measured across the base metal, HAZ, and weld metal. Measurements were obtained at multiple distances from the cap side toward the root side, with a measurement spacing

of 0.5 mm. The hardness recovery distance from the toe of the weld toward the base metal was also evaluated with respect to the 450 HV reference hardness level and the requirements of MIL-STD-1185.

2.5. Ballistic Testing

Ballistic tests were performed at CES Ballistic Test Laboratory according to the FB7 ballistic protection level of EN 1522. The projectile was a 7.62 × 51 mm M61 AP ammunition. Four shots were performed on each welded plate from the distance of 10 m and the velocity of 820 ± 10 m/s: two on the HAZ and two on the weld-metal region. The projectile impact angle was 0°. The ballistic response was evaluated in terms of complete perforation and partial deformation/penetration. After testing, cross-sectional specimens were extracted from the weld and HAZ regions for macrostructural examination of the impact craters, penetration profiles, and damage contours.

3. Results and Discussion

3.1. Macrostructure

No unacceptable surface or volumetric discontinuities were detected during visual, liquid penetrant, or radiographic examination. The welded joints satisfied the applicable acceptance criteria, and no critical cracks, lack of fusion, lack of penetration, or porosity were detected. Macrostructures for different weld groove geometries were presented in Fig. 2. Macrostructural examination also confirmed complete penetration and the absence of significant internal discontinuities. The individual weld passes and HAZ regions were clearly distinguishable. The number of welding passes varied significantly with groove geometry, with the single-V joint requiring 14 passes compared with nine passes for the double-V and double-bevel configurations and ten passes for the single-bevel configuration. The higher number of passes required for the single-V geometry increased the number of repeated thermal cycles experienced by the adjacent HAZ. This effect is important because repeated heating and cooling can modify the morphology of the ICHAZ and alter the distribution of local softening.

In multipass welding, the weld metal consists not only of the columnar region (CR) formed during the solidification of individual weld passes but also of the reheated region (RR), which develops as a result of the tempering effect of subsequent passes. Compared with the columnar region, reheated regions generally exhibit lower hardness and improved toughness, owing to the refinement and tempering of the as-solidified microstructure. This phenomenon has been widely reported in multipass welded joints. Since groove geometry determines both the total weld-metal volume and the bead arrangement, it directly influences the formation and distribution of these two microstructural regions, thereby affecting the mechanical and ballistic performance of the weld metal. Therefore, the surface areas of the weld metal and reheated regions formed under different groove geometries were quantified (Figs. 3a–d), and the corresponding quantitative results are presented in Fig. 3e.

As shown in Fig. 3e, the weld-metal surface area (A_{WM}) was considerably larger in the single-V joint than in the other groove geometries, whereas the double-bevel and single-bevel configurations exhibited the

smallest weld-metal areas. Since undermatched filler metals with lower yield strength than the armor-steel base metal are generally preferred in welded armor structures, a larger weld-metal volume is expected to reduce the overall tensile strength of the welded joint. Accordingly, the lowest joint strength was anticipated for the single-V configuration, whereas the highest strength was expected for the double-bevel configuration. In contrast, ballistic performance depends not only on strength but also on toughness. Because the filler metal used in the present study possesses higher impact toughness than the base armor steel, increasing the weld-metal area is expected to enhance the local energy absorption capacity under projectile impact. It should be noted, however, that the impact toughness of the weld metal is governed not only by its overall volume but also by the relative proportions of the columnar and reheated regions. Therefore, the reheated-region area fraction (A_{RR}%) was also quantified. As shown in Fig. 3e, the highest A_{RR}% values were obtained for the single-bevel and double-bevel groove geometries, whereas the single-V joint exhibited the lowest reheated-region fraction. It should also be noted that the increased weld-metal area is not expected to significantly influence the Charpy V-notch test results, since the notch was positioned entirely within the weld metal for all specimens. However, under ballistic loading, a larger weld-metal surface area increases the probability of direct projectile interaction with the tougher weld metal, which is expected to influence the projectile penetration behavior. This aspect is discussed in detail in the ballistic performance section.

3.2. Microstructural Evaluation

The base metal (BM) consisted predominantly of a tempered martensitic structure (Fig. 4a), consistent with the high strength and hardness of the M450 armor steel. The Heat-affected zone (HAZ) exhibited the characteristic sequence of CGHAZ, FGHAZ, ICHAZ, and SCHAZ regions (Fig. 4b). The CGHAZ was formed near the fusion boundary where the material experienced the highest peak temperatures. The FGHAZ developed at temperatures slightly above the A_3 transformation temperature, while the ICHAZ formed in the intercritical temperature range between A_1 and A_3. The SCHAZ experienced temperatures below A_1 and was primarily affected by tempering rather than complete phase transformation.

The weld-metal microstructures (Fig. 5) consisted predominantly of acicular ferrite (AF) and polygonal ferrite (PF). The double-V (Fig. 5b) and double-bevel (Fig. 5c) joints exhibited the finest AF morphology together with the lowest fraction of PF, which is consistent with their relatively higher weld-metal hardness (Figs. 7c,d). The SEM micrographs further confirmed that the single-V (Fig. 5e) and single-bevel (Fig. 5h) joints contained a considerably higher proportion of PF. In addition to AF, the double-V joint contained a small amount of grain boundary ferrite (GBF). However, the GBF was discontinuously distributed along the prior austenite grain boundaries and its volume fraction was relatively low. Such a morphology is not expected to significantly impair toughness, unlike continuous GBF networks that facilitate crack initiation and propagation.

A comparison of the AF morphology further revealed that the double-bevel joint (Fig. 5g) possessed the finest AF structure among all groove geometries. The single-bevel joint (Fig. 5h) also exhibited a relatively fine AF morphology, which is considered beneficial for maintaining high impact toughness

despite its lower weld-metal hardness. These observations are in good agreement with the Charpy impact test results presented in Table 5. No ferrite side plate (FS(P)) morphology was observed in the weld metal of any groove geometry. The absence of FS(P) indicates that the selected welding conditions and thermal cycles effectively suppressed the formation of coarse ferritic morphologies that are generally associated with reduced impact toughness. Instead, the weld metals were dominated by AF, which is widely recognized as the most desirable ferritic constituent for achieving a favorable combination of strength and toughness in low-alloy steel weld metals.

The CGHAZ and FGHAZ regions generally contained tempered martensite, bainitic constituents, and retained austenite. The microstructures of the ICHAZ were presented in Fig. 6. ICHAZ is particularly important because partial austenitization of the tempered martensitic matrix during intercritical heating, followed by subsequent cooling, promotes the formation of martensite–austenite (M-A) constituents within a softened matrix [11, 12]. During intercritical heating, austenite forms partially within the tempered martensitic matrix, while carbon partitioning from the surrounding matrix enriches the newly formed austenite. Upon subsequent cooling, the carbon-enriched austenite can partially transform into martensite, while the remaining fraction is retained as austenite, resulting in the formation of M-A constituents [18, 28]. The associated carbon redistribution from the surrounding matrix toward the M-A constituents reduces the carbon content of the surrounding matrix and can consequently contribute to a significant decrease in matrix hardness [11, 28]. The volume fraction and morphology of M-A constituents have also been reported to depend strongly on welding heat input. Çoban et al. [11] demonstrated that increasing heat input increased both the size and volume fraction of M-A constituents in the ICHAZ of armor steel, while simultaneously promoting carbon migration from the matrix toward the M-A constituents and reducing matrix hardness. Similar effects of welding thermal conditions on the morphology, size, and fraction of M-A constituents have been reported in high-strength steels [18, 28].

The morphology of the M-A constituents was also influenced by groove geometry since it affects the local thermal cycle. The largest M-A morphology was observed in the central ICHAZ of the single-V joint (Fig. 6a), which also exhibited the lowest local hardness (Fig. 7c). In contrast, the finest M-A morphology was observed in the double-V joint, which exhibited the highest hardness among the corresponding regions. The results indicate that the thermal history generated by the groove geometry played a significant role in determining the morphology of the phases formed in ICHAZ. The repeated thermal cycles associated with the single-V geometry promoted the formation and coarsening of M-A constituents, thereby increasing local softening.

3.3. Hardness Distribution

The horizontal hardness distributions across the welded joints, covering both sides of the weld, were measured along the cap, root, and mid-thickness lines and are presented in Fig. 7a, 7b, and 7c, respectively. In addition, the vertical microhardness distribution through the weld metal is shown in Fig. 7d.

The M450 base metal exhibited hardness values ranging from 456 to 477 HV. In contrast, the average weld-metal hardness values ranged from 277.5 to 303.7 HV, while the average HAZ hardness values ranged from 290.6 to 312.8 HV. The lowest degree of weld-metal softening was obtained with the double-V geometry, corresponding to a softening ratio of approximately 35.17%. The other groove geometries exhibited softening ratios between approximately 38.17% and 39.49%. A similar trend was observed in the HAZ. The double-V geometry exhibited the lowest average softening (approximately 33.22%), whereas the remaining configurations showed softening ratios ranging from approximately 33.22% to 39.08%.

The double-V geometry therefore produced the most favorable overall hardness profile. This behavior is attributed to the more balanced distribution of heat input between both sides of the plate, resulting in a more uniform thermal cycle and consequently reducing excessive softening within the HAZ. However, excessive hardness in the CGHAZ may also be undesirable because it can promote local embrittlement owing to the formation of needle-like martensite under conditions of low heat input and/or excessively rapid cooling [11]. Since groove geometry directly influences the welding sequence and thermal cycle, the localized hardness increase in this region should be evaluated together with the corresponding microstructural evolution. As shown in Fig. 7a, the HAZ hardness in the cap region of the double-V joint slightly exceeded that of the base metal. However, this location corresponded to the FGHAZ, where grain refinement resulted in a moderate hardness increase. Therefore, the observed hardness increase is more likely associated with grain refinement than with the formation of brittle microstructures and is not expected to have a detrimental effect on toughness. The hardness distributions along the root line (Fig. 7b) indicate that, on the right-hand side of the weld, the geometrically similar double-V (X) and double-bevel (K) joints exhibited HAZ hardness values in the CGHAZ and FGHAZ that were only slightly higher than those of the base metal. These increases remained within a reasonable range and were therefore not considered sufficient to adversely affect joint toughness.

When the softening behavior within the ICHAZ–SCHAZ transition region was evaluated, similar hardness values were observed in the cap region for all groove geometries (Fig. 7a). In contrast, a pronounced difference was observed along the root line (Fig. 7b), where the single-V joint exhibited the lowest hardness (approximately 245 HV), whereas the double-V (X) and double-bevel (K) joints maintained substantially higher hardness values of approximately 310 HV. A similar trend was observed at the mid-thickness position (Fig. 7c), although the difference between the groove geometries was less pronounced and no excessive hardness increase was observed.

The vertical hardness profiles measured through the weld metal (Fig. 7d) also revealed higher hardness values for the double-V and double-bevel joints, particularly in the root region. In contrast, the single-V joint exhibited a pronounced hardness reduction near the weld root. The same tendency was also evident in the horizontal hardness distribution measured along the root line (Fig. 7b). These results suggest that the double-V and double-bevel groove geometries are expected to provide higher joint strength but lower ductility than the single-V configuration. This interpretation is consistent with the

tensile test results presented in Fig. 8e, where both geometries exhibited higher yield and tensile strengths accompanied by lower elongation.

According to MIL-STD-1185, the softened region within HAZ of welded armor steels used for military applications should not extend beyond 15.4 mm from any weld toe. In other words, the distance required for the hardness to reach the base-metal hardness level from either weld toe should not exceed 15.4 mm. This requirement aims to minimize the width of the softened HAZ and thereby preserve the ballistic resistance of the welded joint. To evaluate this parameter, hereafter referred to as the hardness recovery distance, the hardness profiles presented in Fig. 7e were analyzed. The hardness recovery distance is primarily governed by the welding heat input and the associated thermal cycle [11, 12]. The hardness recovery distance also varied significantly with groove geometry. The base-metal hardness level of approximately 475 HV was recovered at a distance of approximately 9 mm for the double-bevel (K) joint, 13 mm for the single-bevel (I/) joint, and 14 mm for the double-V (X) joint. In contrast, the single-V (V) joint did not reach the 475 HV hardness level within the maximum allowable distance of 15.4 mm and therefore did not satisfy the requirement specified by MIL-STD-1185. It should be noted, however, that the base-metal hardness measured before welding for the MIL-DTL-46100 Class 2 armor steel used in this study was approximately 456 HV. Therefore, considering the actual hardness of the base material, it can be inferred that the hardness profile of the single-V joint would recover to the original base-metal hardness within the specified 15.4 mm distance. Accordingly, the apparent non-compliance results from adopting the nominal reference hardness of 475 HV rather than the measured hardness of the base metal. Overall, the double-bevel (K) and double-V (X) groove geometries produced the narrowest softened HAZ regions. This finding is particularly significant for armor applications because a wider softened HAZ may provide a preferential path for projectile penetration and subsequent crack propagation, thereby reducing the ballistic resistance of the welded joint.

3.4. Tensile Properties

The average tensile properties are presented in Table 4 and Fig. 8e comparatively.

Table 4
Average tensile properties of the welded joints

Groove geometry	Yield strength (MPa)	Tensile strength (MPa)	Elongation (%)
Single-V	770	865	24
Double-V	800	932	18
Double-bevel	806	959	9
Single-bevel	744	887	16

The double-bevel joint exhibited the highest tensile strength, reaching 959 MPa. However, its elongation was limited to only 9%, indicating a pronounced strength–ductility trade-off. In contrast, the double-V joint achieved a tensile strength of 932 MPa while maintaining an elongation of 18%. Although its tensile

strength was slightly lower than that of the double-bevel joint, it provided the most balanced combination of strength and ductility among the investigated groove geometries.

The average tensile strengths of the single-V, double-V, double-bevel, and single-bevel joints corresponded to joint efficiencies of approximately 56%, 60%, 62%, and 57%, respectively. These values are in good agreement with those reported for welded high-hardness armor steels in the literature. Saxena et al. [22] reported joint efficiencies of approximately 55–63% for welded armor-steel joints, while Gürol et al. [12] and Kurt et al. [7] obtained joint efficiencies generally ranging between 55% and 61% depending on the filler metal and welding conditions. Similar tensile efficiencies have also been reported by Magudeeswaran et al. [13] for quenched-and-tempered armor-steel weldments. Therefore, the tensile performance achieved in the present study is consistent with previously reported values for high-hardness armor steels.

The fracture locations were also consistent with the tensile properties. The single-V joint exhibited the highest elongation, approximately 24%, with fracture occurring in the weld region. The double-V joint exhibited 18% elongation, while the single-bevel joint exhibited 16%. The double-bevel joint exhibited the lowest elongation, 9%, and fracture initiated in the weld metal and subsequently propagated through the HAZ.

These results demonstrate that tensile strength alone is insufficient to identify the optimum groove geometry for armor-steel applications. The double-bevel configuration produced the highest strength but the lowest ductility, whereas the double-V configuration provided a more balanced mechanical response. The tensile behavior was consistent with the hardness distributions discussed previously. The relatively higher weld-metal hardness observed in the double-bevel (K) and double-V (X) joints contributed to their higher tensile strengths. However, the pronounced hardness increase in the double-bevel joint was accompanied by a significant reduction in ductility, whereas the more balanced hardness profile of the double-V joint enabled it to retain considerably higher elongation. In contrast, the lower weld-metal hardness of the single-V joint resulted in lower tensile strength but higher ductility.

3.5. Charpy Impact Toughness

Charpy V-notch impact testing was conducted at − 40°C. The average impact toughness values are presented in Table 5 and Fig. 9.

Table 5
Charpy impact toughness of the weld metal and HAZ at − 40°C

Groove geometry	Weld metal (J)	HAZ (J)
Single-V (V)	69	136
Double-V (X)	53	46
Double-bevel (K)	61	126
Single-bevel (I/)	52	145

The highest weld-metal toughness was obtained for the single-V geometry, with an average value of 69 J. The double-bevel configuration followed with 61 J, while the double-V and single-bevel configurations exhibited values of 53 and 52 J, respectively. The superior weld-metal toughness of the single-V joint is consistent with its lower weld-metal hardness and higher ductility observed during tensile testing. In contrast, the relatively higher hardness of the double-V and double-bevel joints resulted in lower absorbed impact energies, reflecting the well-established inverse relationship between hardness and impact toughness.

The HAZ impact toughness exhibited a markedly different trend. The single-bevel joint exhibited the highest HAZ toughness (145 J), followed by the single-V and double-bevel joints with values of 136 and 126 J, respectively. In contrast, the double-V joint absorbed only 46 J. This result indicates that the impact behavior of the HAZ was governed primarily by the local microstructural evolution associated with the thermal cycle generated by the groove geometry rather than by hardness alone. Although the double-V joint exhibited the most favorable hardness distribution and tensile response, its HAZ exhibited the lowest impact toughness. This observation suggests that impact toughness is influenced not only by hardness but also by local grain morphology, crack initiation behavior, phase distribution, and other microstructural features developed during multipass welding.

The differences between the weld-metal and HAZ toughness trends demonstrate that groove geometry affects different regions of the welded joint through different metallurgical mechanisms. While the weld metal was primarily influenced by the solidification microstructure and weld-metal hardness, the HAZ response depended largely on the local thermal cycle and the resulting phase transformations. Consequently, no direct correlation was observed between hardness and impact toughness in every region of the welded joint.

3.6. Ballistic Performance

Ballistic testing was performed according to the FB7 protection level specified in EN 1522 using 7.62 × 51 mm M61 AP ammunition. Four shots were applied to each welded plate, including two shots in the HAZ and two in the weld-metal (WM) region. The ballistic test results are presented in Table 6 and Fig. 10, which includes the projectile impact locations and corresponding Width of Penetration (WoP) measurements for the WM and HAZ (Fig. 10a), a comparative evaluation of the Depth of Penetration

(DoP) and WoP values (Fig. 10b), and macrographs of the welded-joint cross-sections after ballistic testing showing the projectile penetration depths in both the WM and HAZ (Fig. 10c). All welded joints successfully resisted complete perforation, and only localized plastic deformation together with partial projectile penetration was observed. Consequently, all welded joints with varying groove geometries resisted complete perforation under the applied FB7 test conditions under the applied test conditions.

Table 6
Measured DoP and WoP values for WM and HAZ of joints with different groove geometries

Groove geometry	Weld metal		HAZ	
	DoP	WoP	DoP	WoP
Single-V (V)	16	15.16 / 16.26	20	13.62 / 13.92
Double-V (X)	20	18.84 / 13.87	15	15.89 / 13.88
Double-bevel (K)	20	18.39 / 14.85	10,5	16.54 / 16.75
Single-bevel (I/)	20	14.41 / 14.37	11,5	15.48 / 16.13

Although all joints fulfilled the ballistic requirements, the penetration characteristics varied considerably with groove geometry. The HAZ exhibited the greatest penetration depth in the single-V joint, which also possessed the widest softened region and the longest hardness recovery distance. Conversely, the double-bevel (K) and single-bevel (I/) joints exhibited the lowest HAZ penetration depths, consistent with their narrower softened regions and shorter hardness recovery distances. These findings indicate that the extent of HAZ softening plays a dominant role in controlling local ballistic resistance by promoting projectile-induced plastic deformation and crack propagation.

A different trend was observed in the weld metal. The single-V joint exhibited the lowest DoP (16 mm), whereas the remaining groove geometries exhibited identical DoP values of approximately 20 mm. This behavior is attributed to the combination of the relatively lower weld-metal hardness, higher weld-metal toughness, and the larger weld-metal surface area exposed to projectile impact in the single-V configuration, as discussed previously in Fig. 3. The larger exposed weld-metal area enabled a greater proportion of the projectile to interact with the tougher weld metal rather than the adjacent HAZ, thereby reducing penetration depth. Similar observations have been reported in our previous study on sandwich armor joints and by Naveen Kumar et al., who showed that tougher weld metals produced lower DoP values, whereas harder weld metals restricted lateral plastic deformation, resulting in lower WoP values [21, 29]. This relationship is also evident in the present study (Fig. 10b), where an inverse correlation between DoP and WoP can generally be observed. Weld regions exhibiting lower penetration depths tended to produce larger penetration widths, whereas deeper projectile penetration was generally accompanied by smaller WoP values. This behavior reflects the different energy absorption mechanisms of softer/tougher and harder weld metals, where the former promote greater plastic deformation while the latter constrain lateral deformation.

Overall, the results demonstrate that the governing ballistic mechanisms differ fundamentally between the weld metal and the HAZ. In the HAZ, ballistic performance was governed primarily by the extent of local softening and the hardness recovery distance. In contrast, the weld-metal response depended predominantly on the balance between hardness, toughness, and the effective weld-metal area subjected to projectile impact. Consequently, the optimum groove geometry for maximizing ballistic performance in the weld metal is not necessarily the same as that for the HAZ, highlighting the importance of evaluating these regions independently when designing welded armor structures.

4. Conclusions

This study systematically investigated the influence of four different groove geometries (single-V, double-V, single-bevel, and double-bevel) on the microstructure, hardness distribution, tensile properties, impact toughness, and ballistic performance of 20 mm thick M450 armor steel welded by the GMAW process. Based on the experimental results, the following conclusions can be drawn:

- Groove geometry significantly affected the thermal cycle experienced by the welded joint, resulting in distinct microstructural evolution, hardness distributions, and softened HAZ characteristics. The morphology of the M-A constituents in the ICHAZ, the hardness recovery distance, and the extent of HAZ softening were found to be strongly dependent on groove design.
- Among the investigated configurations, the double-V groove produced the most balanced hardness profile by minimizing ICHAZ softening while avoiding excessive hardening in the CGHAZ. Furthermore, its hardness recovery distance satisfied the MIL-STD-1185 requirement, indicating a relatively narrow softened HAZ.
- The double-bevel joint exhibited the highest tensile strength (959 MPa), whereas the single-V joint showed the greatest ductility and weld-metal impact toughness. The double-V configuration provided the most balanced combination of tensile strength, ductility, and hardness distribution, demonstrating that tensile strength alone is insufficient for selecting the optimum groove geometry for armor-steel applications.
- Ballistic performance was governed by different mechanisms in the weld metal and the HAZ. In the HAZ, projectile penetration was primarily controlled by the extent of local softening and the hardness recovery distance. Groove geometries producing narrower softened regions exhibited lower penetration depths and improved local ballistic resistance.
- In contrast, the ballistic response of the weld metal was controlled predominantly by the combined effects of weld-metal hardness, impact toughness, and the effective weld-metal area exposed to projectile impact. The single-V configuration exhibited the lowest weld-metal penetration depth despite its lower hardness, confirming that increased weld-metal toughness can effectively improve local resistance against projectile penetration.
- An inverse relationship between the Depth of Penetration (DoP) and Width of Penetration (WoP) was observed. Weld regions exhibiting lower DoP generally produced greater WoP owing to enhanced

plastic deformation, whereas harder regions restricted lateral deformation and resulted in narrower but deeper penetration profiles.

Overall, the results demonstrate that groove geometry is a critical design parameter influencing not only weldability and mechanical performance but also the ballistic behavior of welded armor structures. Since the governing penetration mechanisms differ fundamentally between the weld metal and the HAZ, the optimum groove geometry for maximizing ballistic performance cannot be selected on the basis of a single mechanical property. Instead, groove design should be optimized by simultaneously considering thermal history, microstructural evolution, hardness distribution, and the distinct ballistic responses of both the weld metal and the heat-affected zone. The findings provide a practical framework for selecting groove geometries in thick welded armor structures by linking welding design directly to ballistic performance through microstructural evolution and hardness distribution.

Declarations

Competing Interests

The authors declare that they have no competing interests. We declare that we do not have any commercial or associative interest that represents a competing interest in connection with the work submitted.

Funding

This work was supported by the Scientific and Technological Research Council of Türkiye (TÜBİTAK) under Project No: 5210029.

Acknowledgments

This work was supported by the Scientific and Technological Research Council of Türkiye (TÜBİTAK) under Project No. 5210029. This paper is based on the M.Sc. thesis entitled "Investigation of the Effect of Weld Groove Design on the Microstructure and Mechanical Properties of High-Strength Ballistic Armor Steels" (Thesis No. 999447) by Müesser Göçmen, submitted to the Graduate School of Istanbul Gedik University.

Data Availability

The data supporting the findings of this study are available from the corresponding author upon reasonable request.

References

1. Afkhami S, Björk T, Larkiola J (2019) Weldability of cold-formed high strength and ultra-high strength steels. J Constr Steel Res 158:86–98. https://doi.org/10.1016/j.jcsr.2019.03.017
2. Hanhold B, Babu SS, Cola G (2013) Investigation of heat affected zone softening in armour steels: Part 2—Mechanical and microstructure heterogeneity. Sci Technol Weld Join 18:253–260. https://doi.org/10.1179/1362171812Y.0000000101
3. Magudeeswaran G, Balasubramanian V, Madhusudhan Reddy G (2018) Metallurgical characteristics of armour steel welded joints used for combat vehicle construction. Def Technol 14:590–606. https://doi.org/10.1016/j.dt.2018.07.021
4. Robledo DM, Gómez JAS, Giraldo JEG (2011) Development of a welding procedure for MIL A 46100 armor steel joints using gas metal arc welding. Dyna 78:65–71
5. Garašić I, Jurica M, Iljkić D, Barišić A (2019) Determination of ballistic properties on ARMOX 500T steel welded joint. Eng Rev 39:186–196. https://doi.org/10.30765/er.39.2.8
6. Morsy MA, Abdel Aziz SM, Abdelwahed K, Abdelwahab SA (2022) Effect of welding parameters on the mechanical and metallurgical properties of armor steel weldment. J Eng Appl Sci 69. https://doi.org/10.1186/s44147-022-00102-7
7. Kurt RM, Gürol U, Tümer M (2026) Microstructural and mechanical characterization of robotic-MAG welded armor-grade steel: Effect of filler metal selection. Weld World. https://doi.org/10.1007/s40194-026-02391-5
8. Çelik C, Gürol U (2025) Impact of sandwich joint on mechanical and ballistic performance of high-hardness armor steels. Weld World 69:3031–3052. https://doi.org/10.1007/s40194-025-02023-4
9. Çoban O, Göçmen M, Çelik C, Baykal H, Gürol U, Koçak M (2023) Yüksek mukavemetli balistik zırh çeliklerinin kaynaklanabilirliği. Uludağ Univ Müh Fak Derg 28:1009–1028. https://doi.org/10.17482/uumfd.1333002
10. Hanhold B, Babu SS, Cola G (2013) Investigation of heat affected zone softening in armour steels: Part 1—Phase transformation kinetics. Sci Technol Weld Join 18:247–252. https://doi.org/10.1179/1362171812Y.0000000100
11. Çoban O, Kaymak F, Gürol U, Koçak M (2023) Characterization of fillet welded armor steel performed by robotic gas metal arc welding: Effect of heat input on microstructure and microhardness. J Mater Eng Perform. https://doi.org/10.1007/s11665-023-09058-y
12. Gürol U, Karahan T, Erdöl S, Çoban O, Baykal H, Koçak M (2022) Characterization of armour steel welds using austenitic and ferritic filler metals. Trans Indian Inst Met 75:757–770. https://doi.org/10.1007/s12666-021-02464-7
13. Magudeeswaran G, Balasubramanian V, Balasubramanian TS, Reddy GM (2008) Effect of welding consumables on tensile and impact properties of shielded metal arc welded high strength, quenched and tempered steel joints. Sci Technol Weld Join 13:97–105. https://doi.org/10.1179/174329307X249432
14. Serrano R, Ambriz RR, Ayoub G, Jaramillo D (2022) Mechanical behavior of armor steel gas metal arc welding joints performed by nickel-chromium and low-alloy steel filler metals. J Mater Eng

Perform 31:3930–3942. https://doi.org/10.1007/s11665-021-06517-2

15. Kumar SN, Balasubramanian V, Malarvizhi S, Rahman AH, Balaguru V (2022) Effect of welding consumables on shielded metal arc welded ultra-high hard armour steel joints. J Mech Behav Mater 31:8–21. https://doi.org/10.1515/jmbm-2022-0002
16. Balaguru V, Balasubramanian V, Sivakumar P (2020) Effect of weld metal composition on impact toughness properties of shielded metal arc welded ultra-high hard armor steel joints. J Mech Behav Mater 29:186–194. https://doi.org/10.1515/jmbm-2020-0019
17. Bhadeshia HKDH (2013) About calculating the characteristics of the martensite–austenite constituent. In: Proceedings of the International Seminar on Welding of High Strength Pipeline Steels, pp 99–106. CBMM and The Minerals, Metals & Materials Society
18. Wang XL, Nan YR, Xie ZJ, Tsai YT, Yang JR, Shang CJ (2017) Influence of welding pass on microstructure and toughness in the reheated zone of multi-pass weld metal of 550 MPa offshore engineering steel. Mater Sci Eng A 702:196–205. https://doi.org/10.1016/j.msea.2017.06.081
19. Savic B, Cabrilo A (2021) Effect of heat input on the ballistic performance of armor steel weldments. Materials 14:3617. https://doi.org/10.3390/ma14133617
20. Souza ERS, Weber RP, Monteiro SN, Oliveira SA (2021) Microstructure effect of heat input on ballistic performance of welded high strength armor steel. Materials 14:5789. https://doi.org/10.3390/ma14195789
21. Kumar SN, Balasubramanian V, Malarvizhi S, Rahman AH, Balaguru V (2022) Effect of failure modes on ballistic performance of gas metal arc welded dissimilar armour steel joints. CIRP J Manuf Sci Technol 37:570–583. https://doi.org/10.1016/j.cirpj.2022.03.004
22. Saxena A, Dwivedi SP, Sharma S, Srivastava VS, Singh G, Singh J et al (2021) A comparative numerical analysis on the effect of welding consumables on the ballistic resistance of SMAW joints of armor steel. Appl Sci 11:3629. https://doi.org/10.3390/app11083629
23. Cabrilo A, Cvetinov M (2017) Fatigue crack propagation and Charpy impact properties in armor steel welds. Mater Plast 54:694–699. https://doi.org/10.37358/MP.17.4.4927
24. Kumar S et al (2014) Effect of groove design on mechanical and metallurgical properties of quenched and tempered low alloy abrasion resistant steel welded joints. Mater Des 53:727–736. https://doi.org/10.1016/j.matdes.2013.07.043
25. İpek NE, Elaldi F (2012) Analysis of welding groove angle and geometry on strength of armor steel. Mater Manuf Process 27:1437–1441. https://doi.org/10.1080/10426914.2012.709343
26. Kim JS, Yi HJ (2017) Characteristics of GMAW narrow gap welding on the armor steel of combat vehicles. Appl Sci 7:658. https://doi.org/10.3390/app7070658
27. Vimal Kumar N, Uthayakumar M, Thirumalai Kumaran S, Velayudham A (2022) The effect of weld-groove surface modification on the joint performance of military grade armour steel: A sustainability approach. Mater Chem Phys 281:125902. https://doi.org/10.1016/j.matchemphys.2022.125902
28. Moreira de Oliveira DF, de Faria GL, Porcaro RR (2026) Peak temperature and cooling rate effects on M–A constituent characteristics in the ICCGHAZ of HSLA steels: A review. Weld World.

https://doi.org/10.1007/s40194-026-02429-8
29. Gürol U, Çelik C, Çoban O, Göçmen M, Koçak M (2025) Mechanical and ballistic performance of high-hardness armor steels welded with ASS-LHF sandwich joint design. Mater Today Commun 42:111209. https://doi.org/10.1016/j.mtcomm.2024.111209

Figures

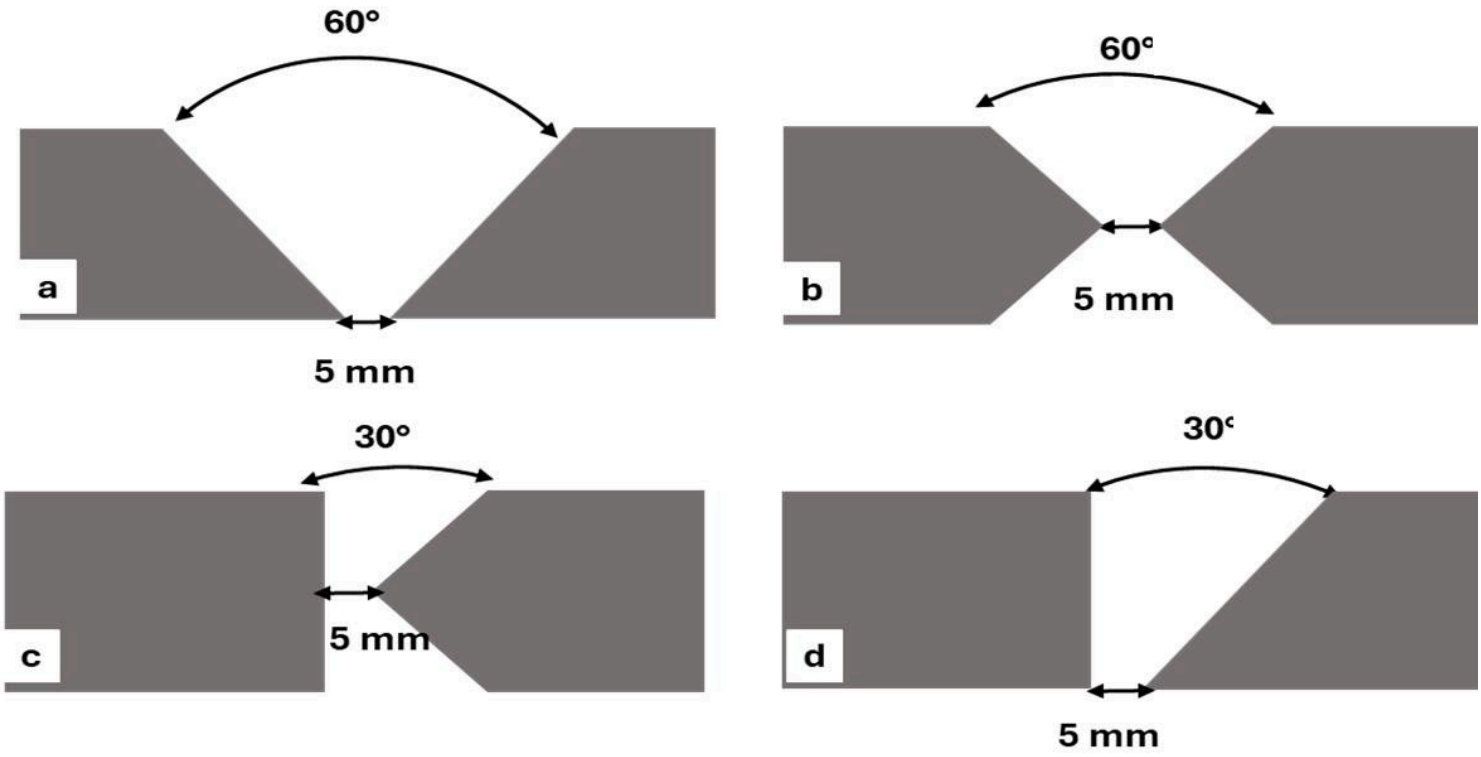


Figure 1

Schematic representation of weld groove design (a) single-V (V), (b) double-V (X), (c) double-bevel (K), (d) single-bevel (I/)

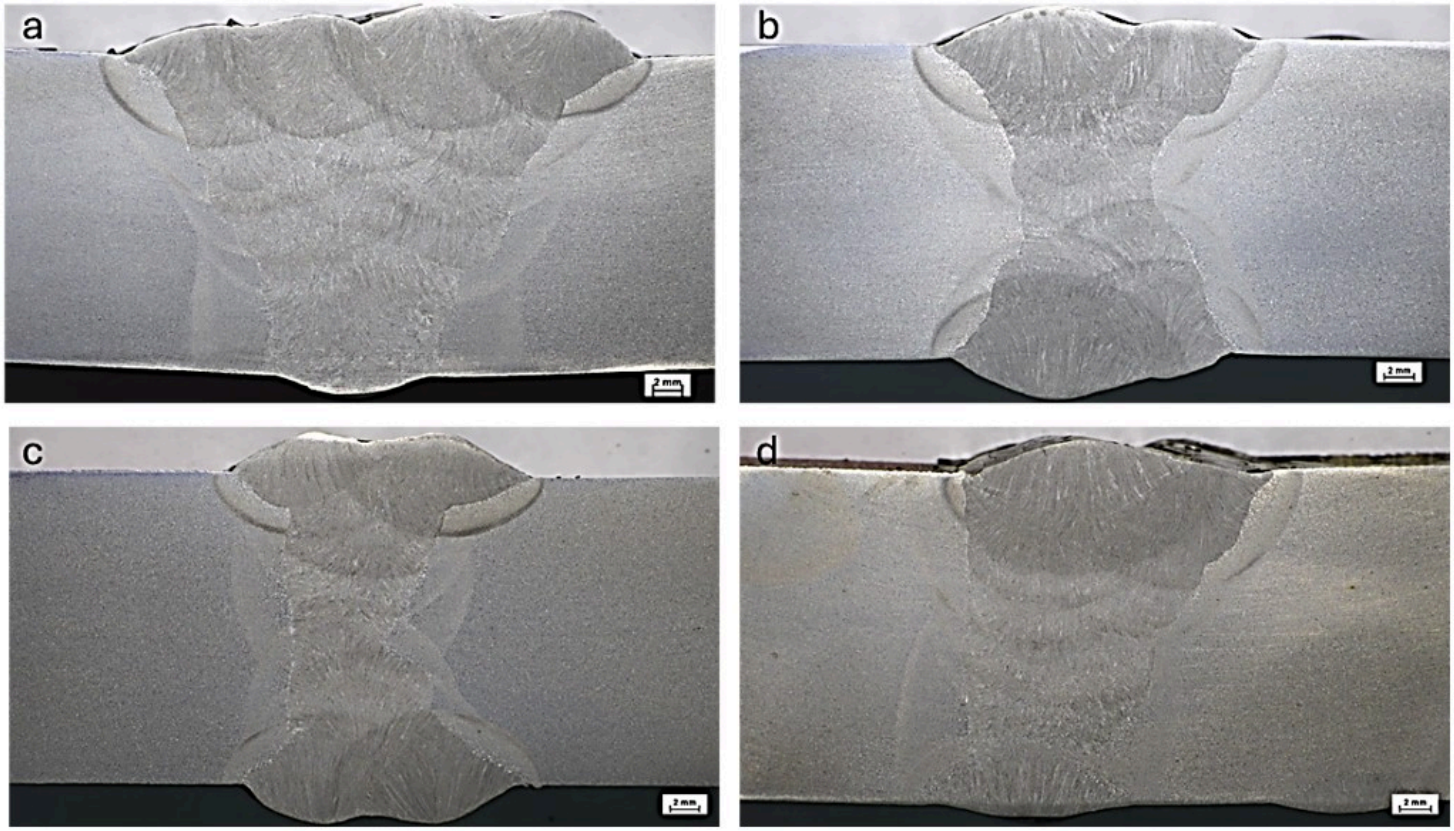


Figure 2

Macrostructure of weld joints for (a) single-V (V), (b) double-V (X), (c) double-bevel (K), (d) single-bevel (I/)

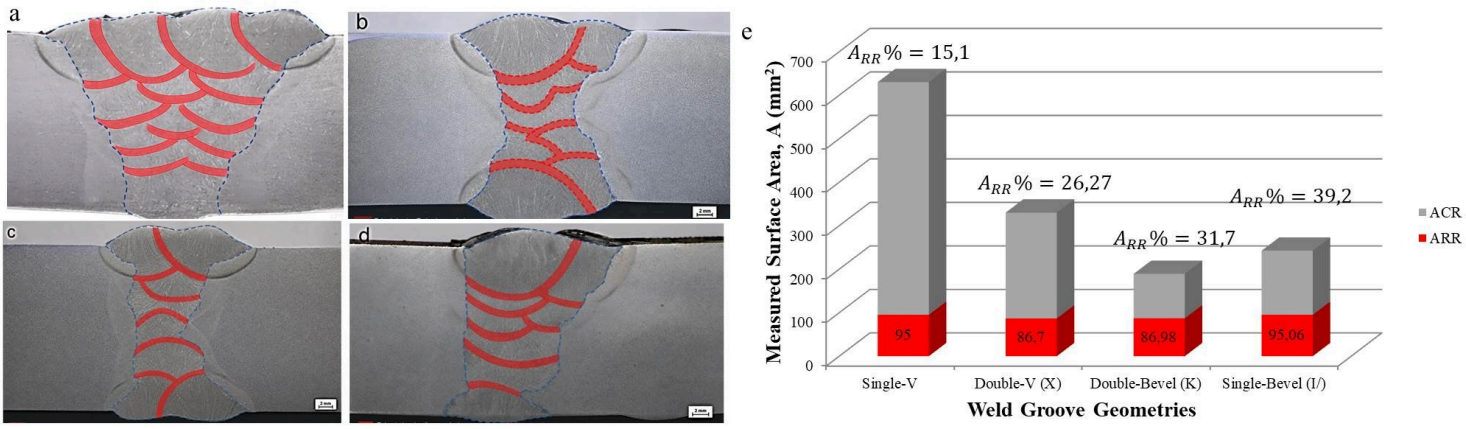


Figure 3

Macrostructures showing reheated regions (highlighted areas) and weld metal edges (dashed lines) for (a) single-V (V), (b) double-V (X), (c) double-bevel (K), (d) single-bevel (I/) and (e) surface area measurements in weld metal

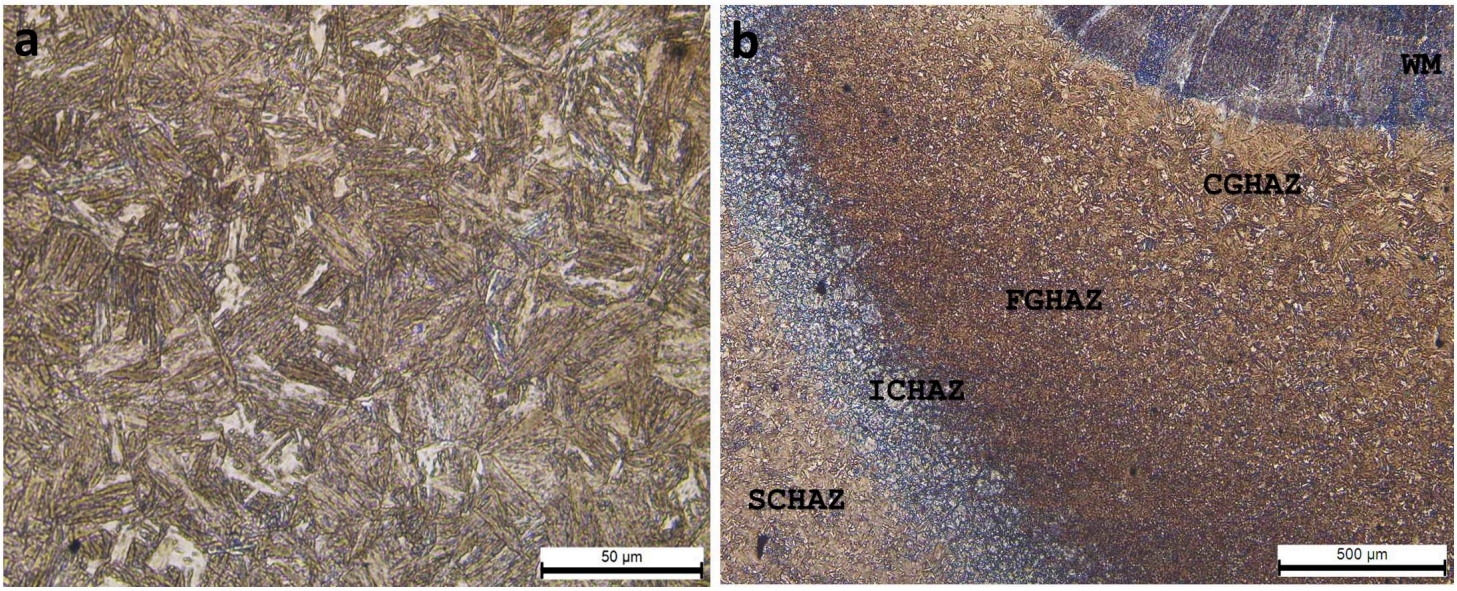


Figure 4

Microstructure of (a) BM and (b) HAZ

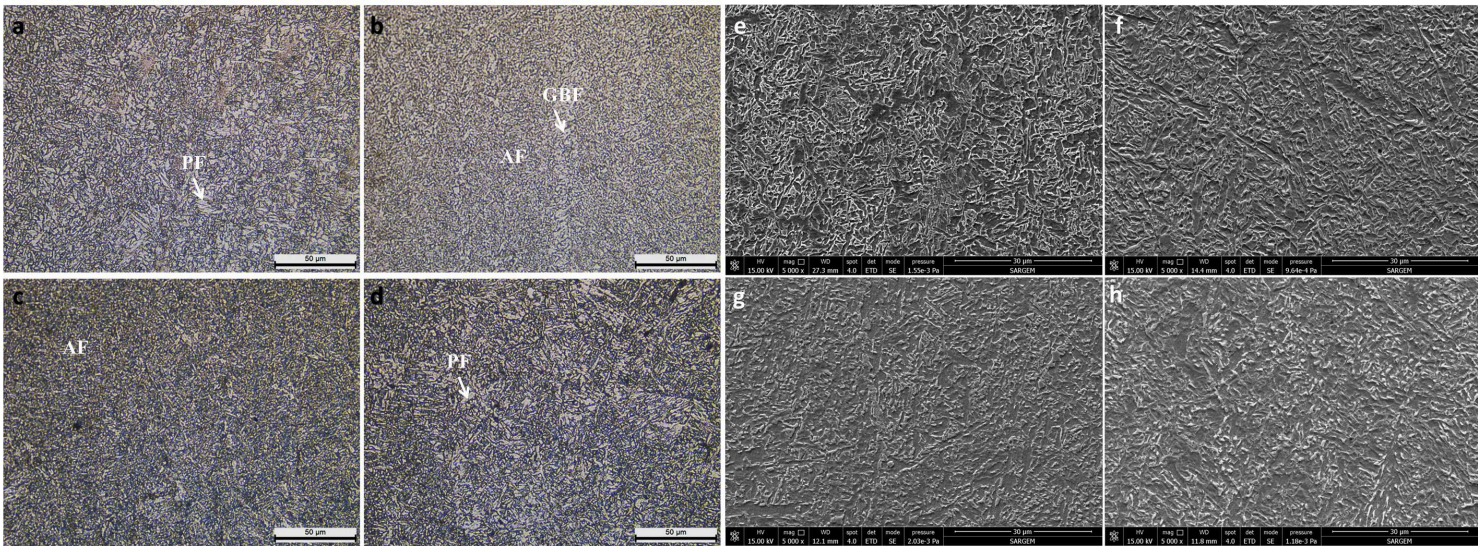


Figure 5

Microstructures and SEM micrographs of weld metal center for (a), (e) single-V (V), (b), (f) double-V (X), (c), (g) double-bevel (K), (d), (h) single-bevel (I/)

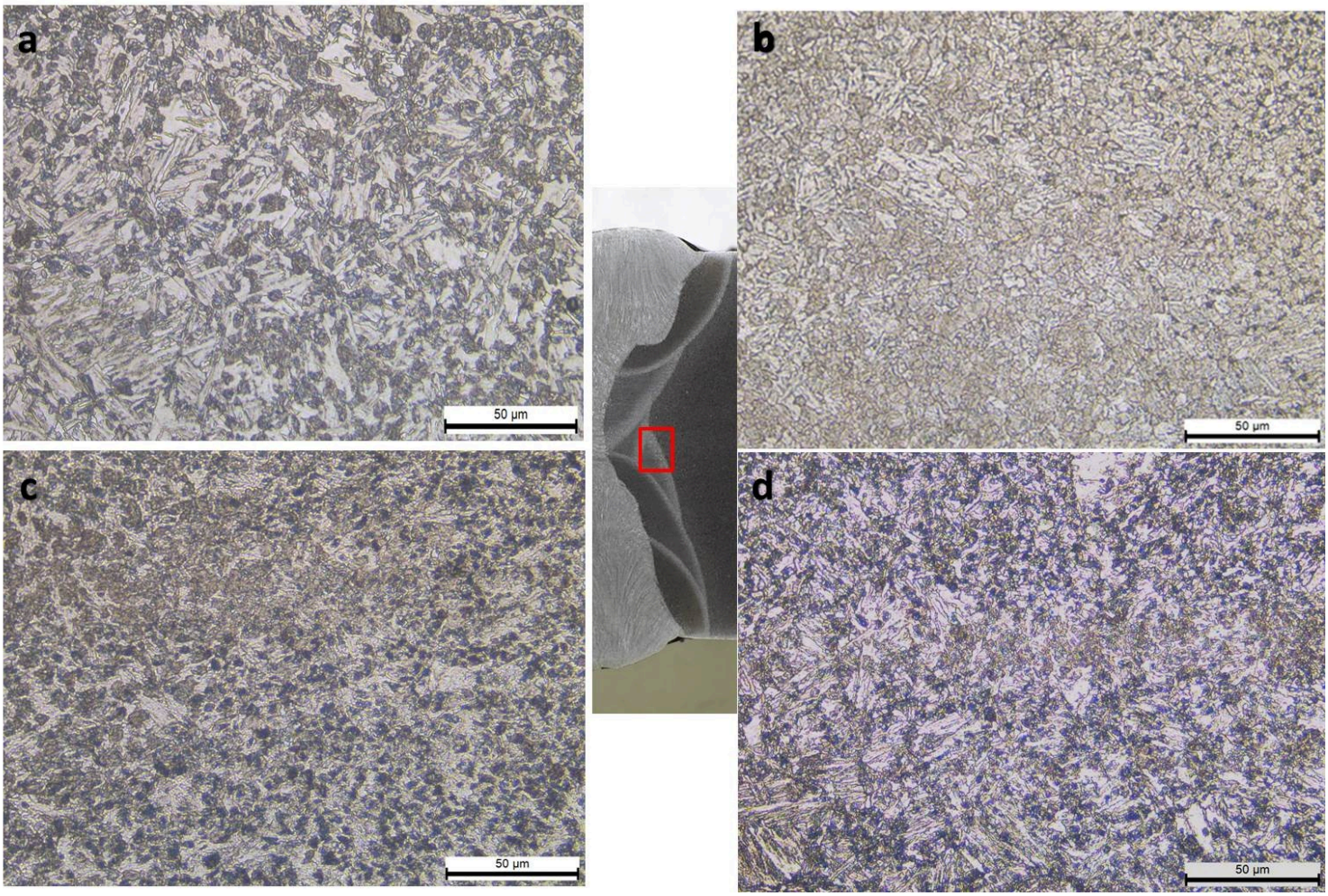


Figure 6

Microstructures of central ICHAZ for (a) single-V (V), (b) double-V (X), (c) double-bevel (K), (d) single-bevel (I/)

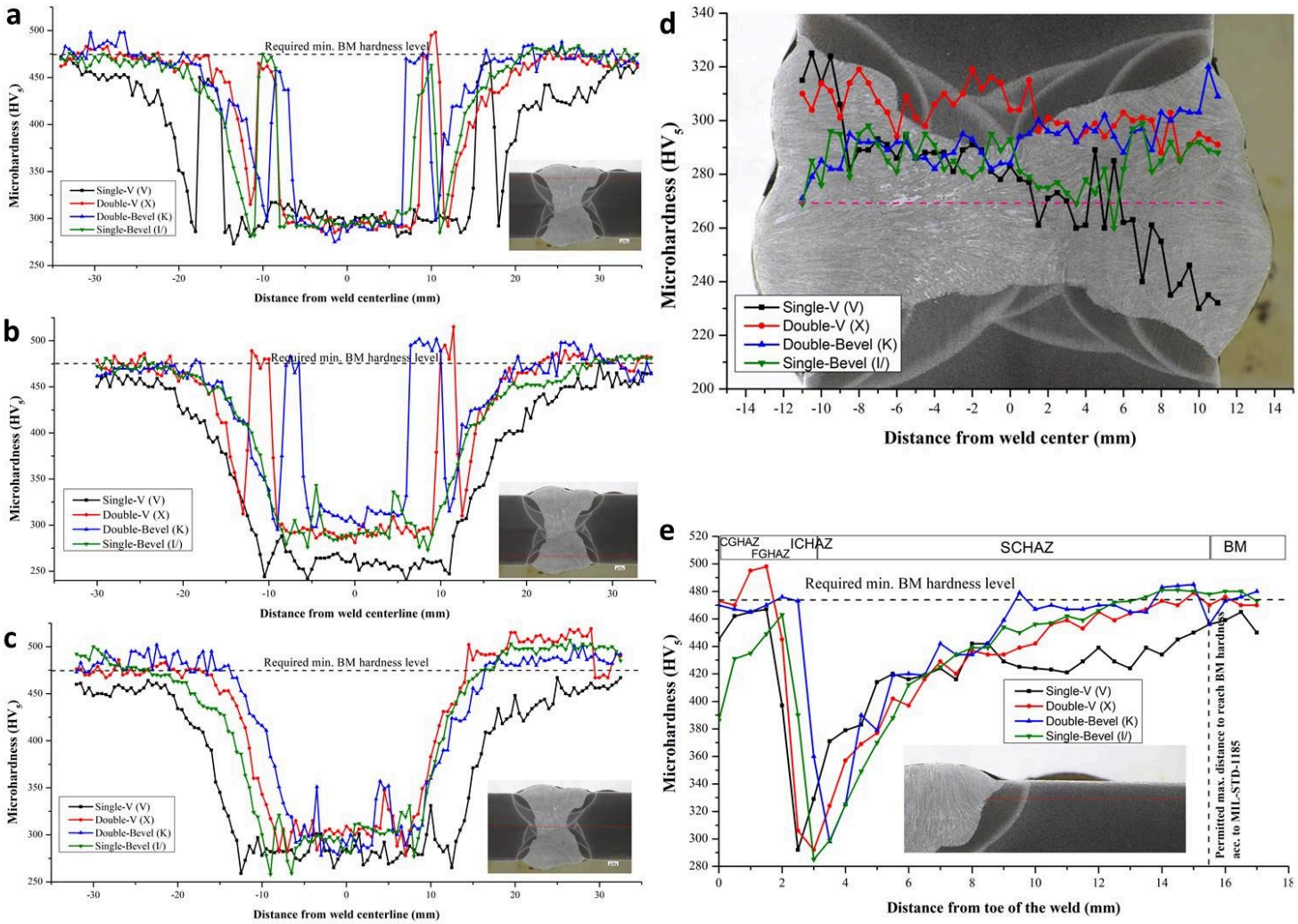


Figure 7

Microhardness test results (a) cap, (b) root, (c) middle, (d) weld metal, (e) HAZ hardness distribution for MIL-STD-1185 evaluation

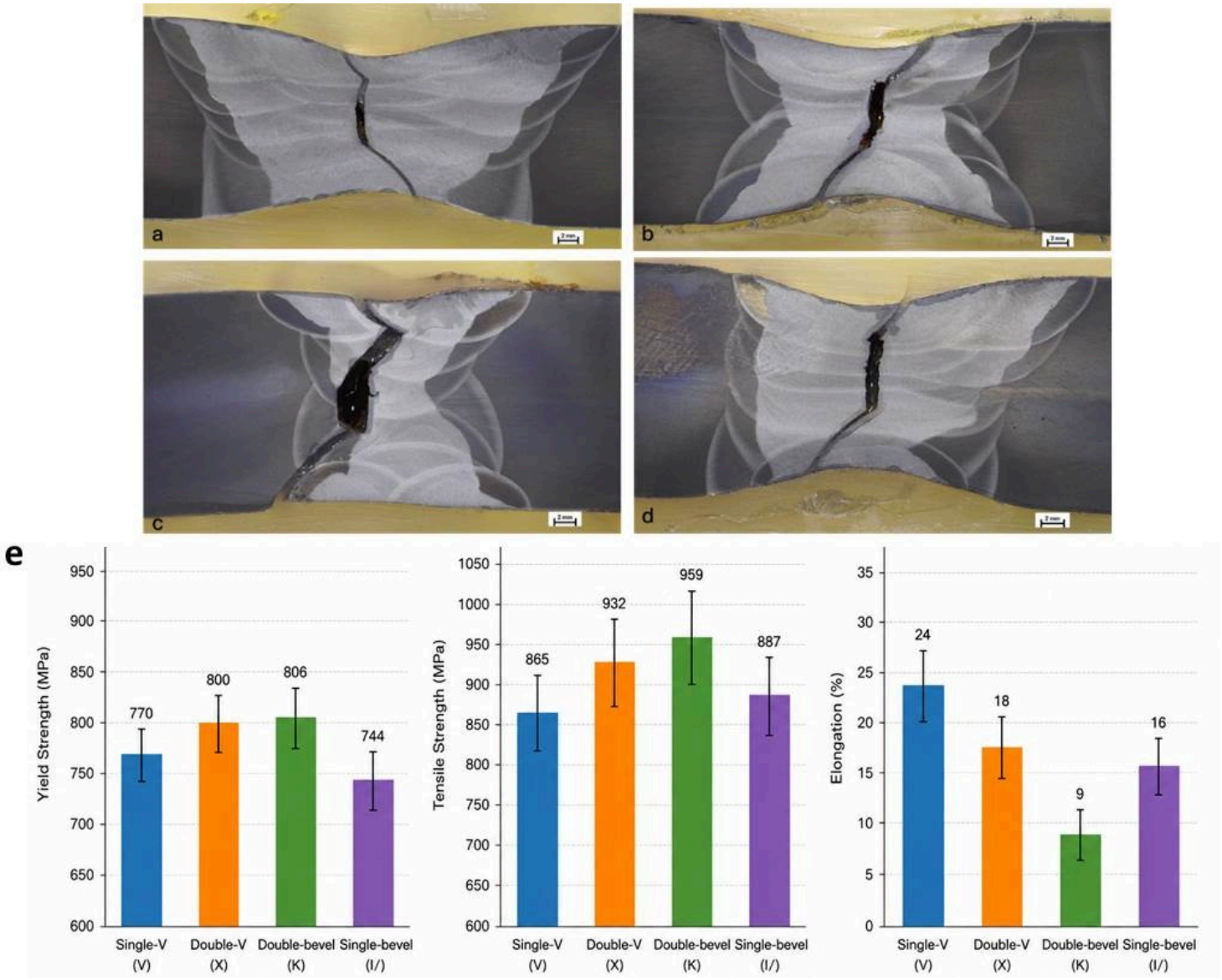


Figure 8

Macro view of tensile specimens showing fracture locations for (a) single-V (V), (b) double-V (X), (c) double-bevel (K), (d) single-bevel (I/), and (e) Tensile properties of welded joints

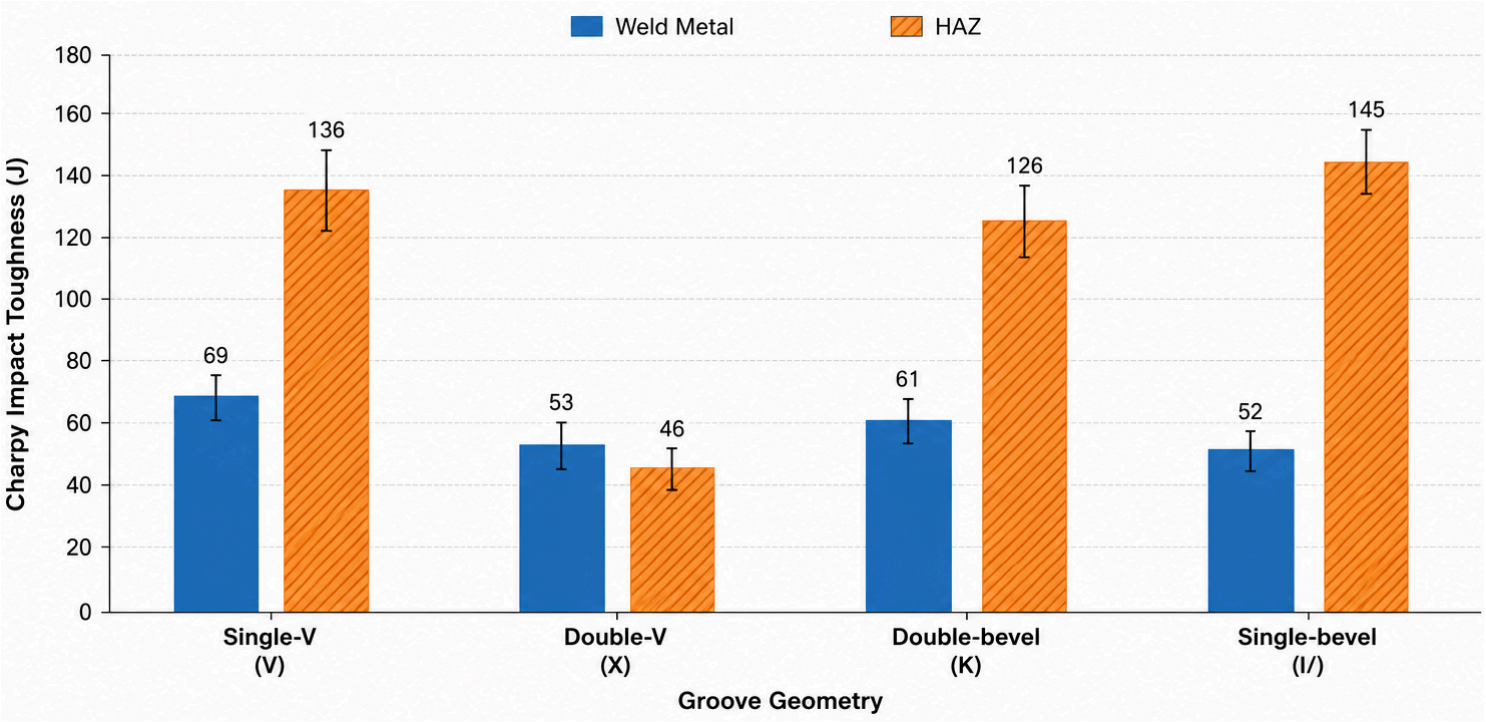


Figure 9

Charpy-V impact test results at -40 ^{0}C

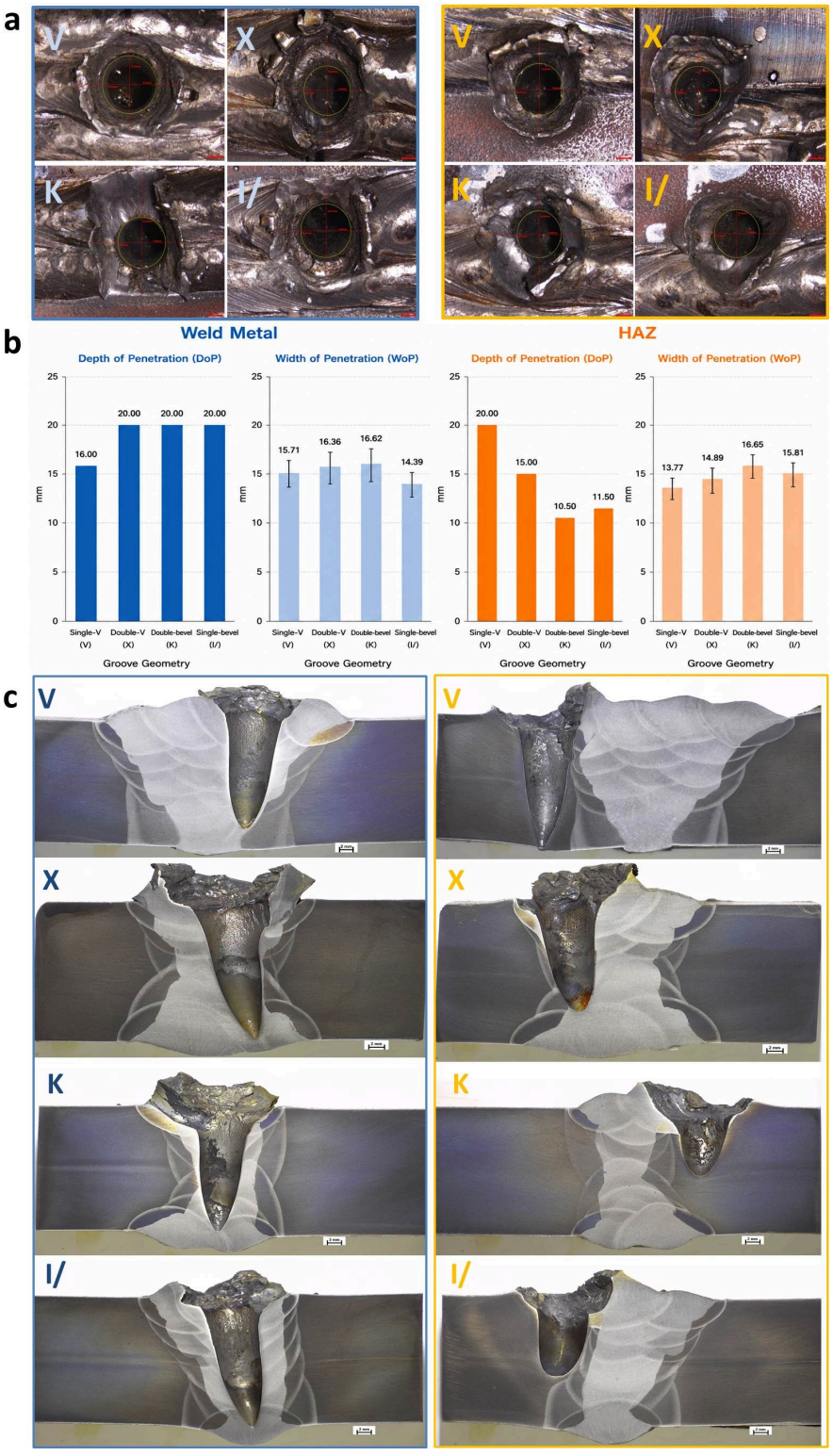


Figure 10

Ballistic test results, (a) views of projectile impact locations showing WoP measurements for WM and HAZ, (b) comparative results for DoP and WoP, (c) macro view of cross-section of welded joints after ballistic tests, showing DoP of projectile for WM and HAZ